Atomic data and solar spectral diagnostics, from the X-rays to the near infrared

Giulio Del Zanna

Roger P. Dufresne

DAMTP, University of Cambridge (UK)

See Living Review (Del Zanna & Mason 2018, Springer)

Science & Technology Facilities Council

Del Zanna G, Solvay workshop, Brussels Nov 2019

UNIVERSITY OF CAMBRIDGE

Atomic data for astrophysics

SCATTERING CALCULATIONS:

UK APAP Network http://www.apap-network.org/
funded by STFC has become the main ion atomic data provider for fusion and astrophysics (cf. Badnell+2017, Mao+poster)

STRUCTURE CALCULATIONS:

COMPAS group (GRASP2K)
cf. Jonsson+2017, K.Wang poster

BENCHMARK:

line identifications (novel) and benchmark

DISTRIBUTION:
CHIANTI (www.chiantidatabase.org), with over 3000 citations, main database for ions.

Common open-data policy on published codes and atomic data.

Non-thermal electrons ?

Using UK-APAP cross-sections, we found evidence of non-Maxwellian e in AR using EUV Hinode EIS spectra (cf. Dudik+2017 review).
Best diagnostics are in the X-rays

CHIANTI v.9 (Dere, Del Zanna et al. 2019) includes main Li-like ions + satellites of Fe ions

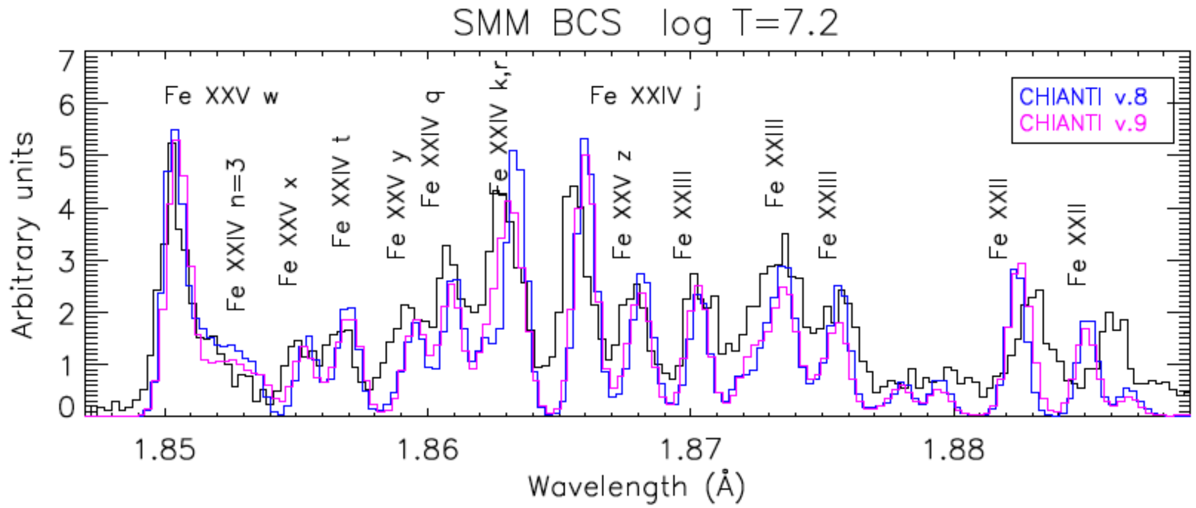

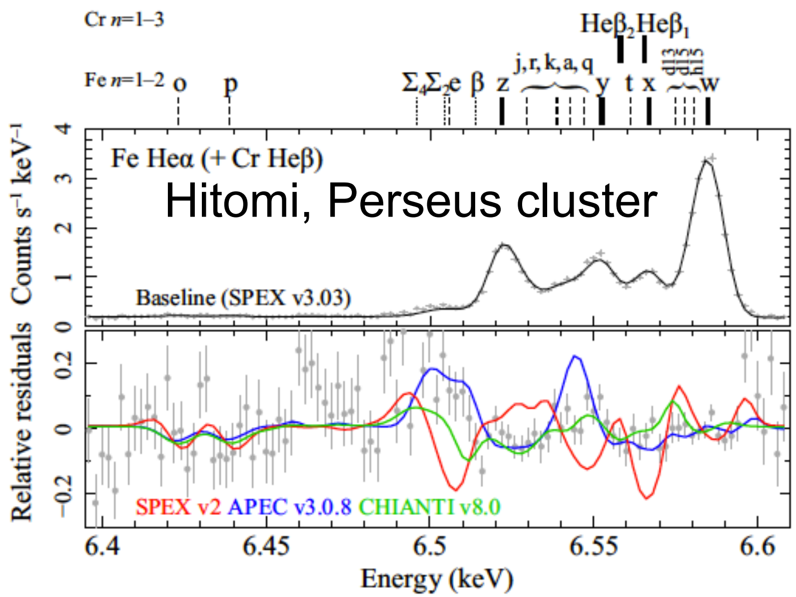

Relevant for Hitomi follow-up and Athena

ov 2019

CHIANTI v.9

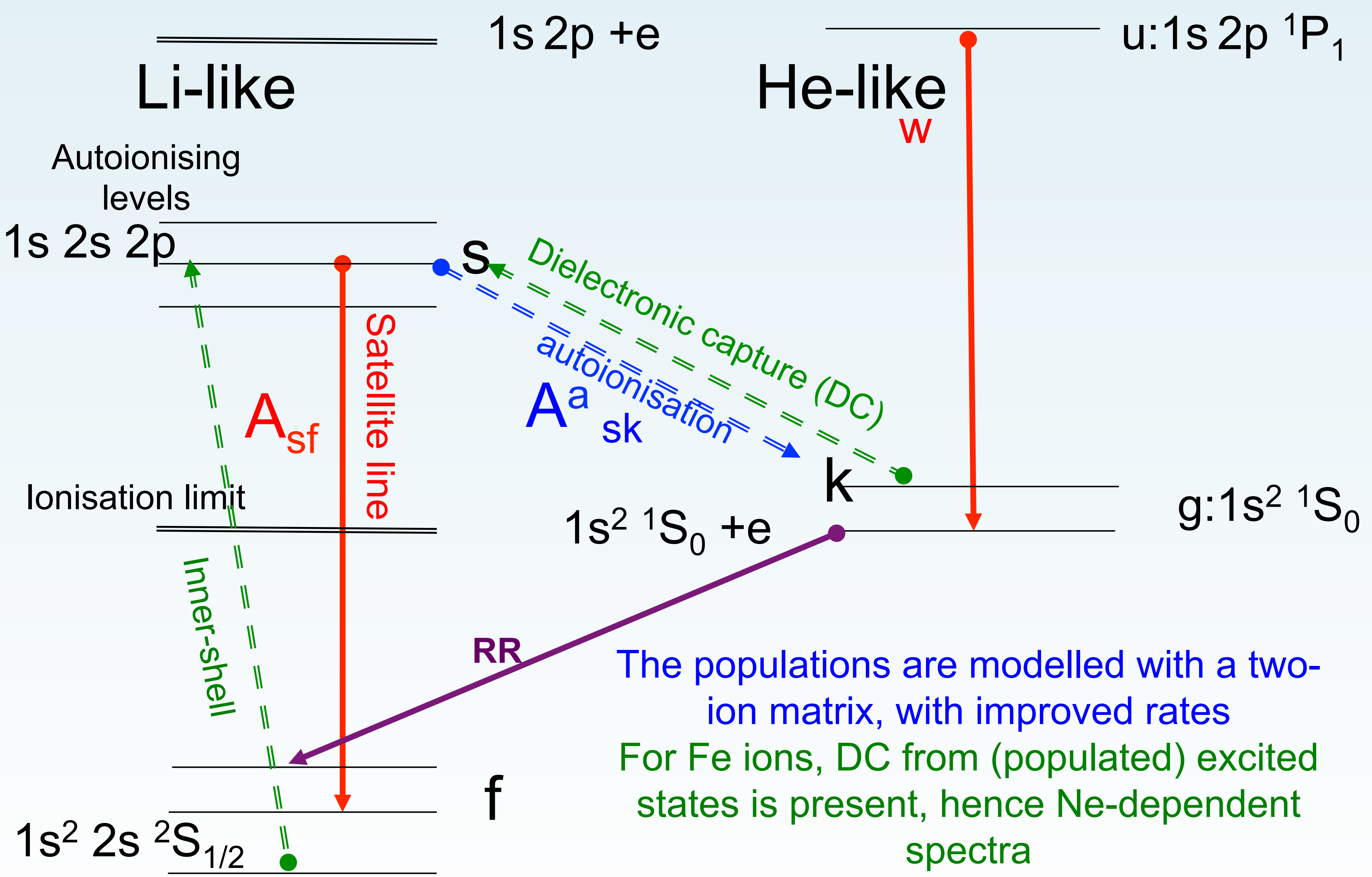

The populations are modelled with a two-ion matrix, with improved rates

For Fe ions, DC from (populated) excited states is present, hence Ne-dependent spectra

Te from line ratios – same ion

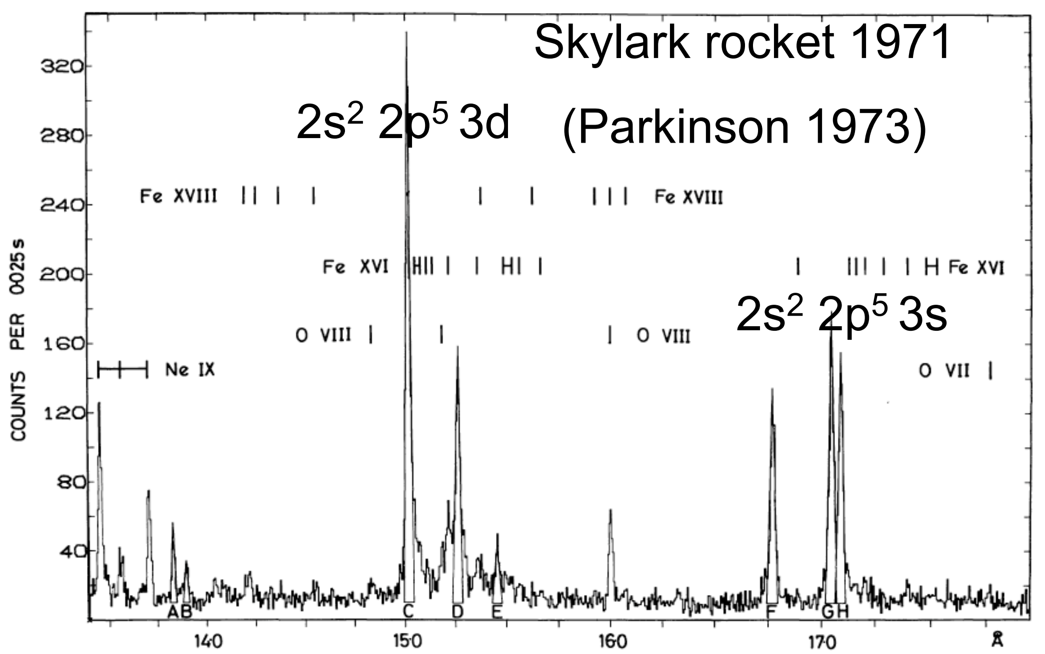

Many examples of 'new' diagnostics in the X-rays and EUV, where excitation rates make a difference of factors ~2

2020: first X-ray imaging spectroscopy with a sounding rocket (MaGIXS)

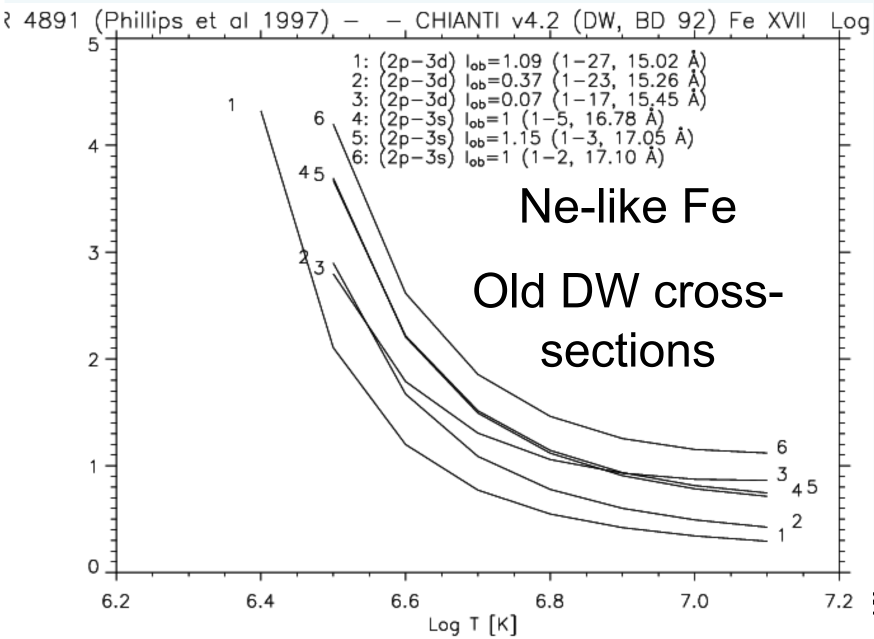

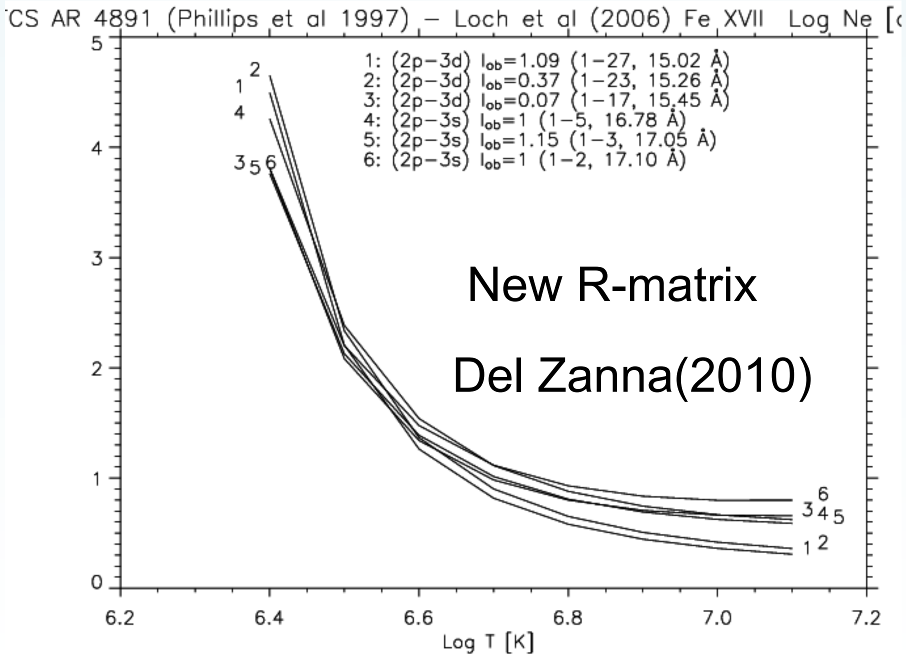

Heating in solar active regions ?

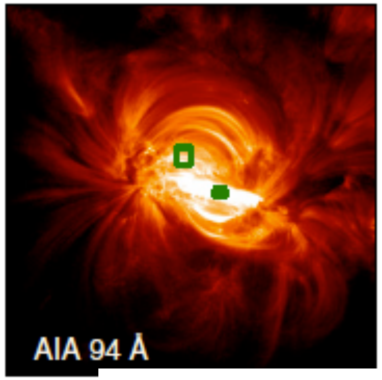

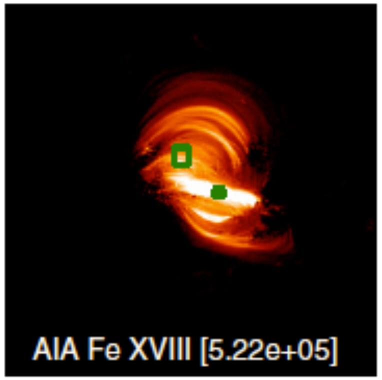

SDO AIA 94 Å images show ubiquitous presence of Fe XVIII (e.g. Warren et al. 2012)
7 MK plasma in active regions !?

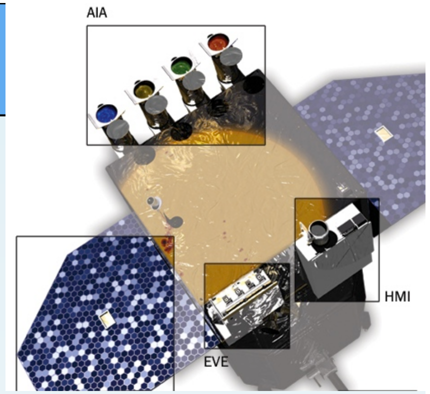

NASA SDO

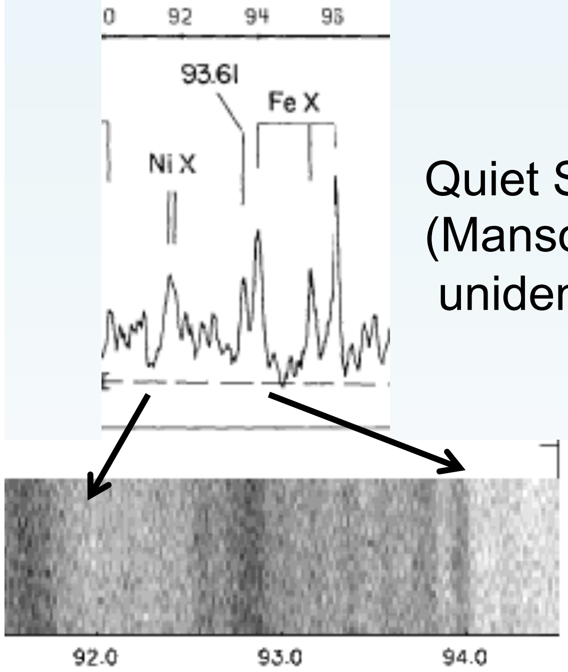

Quiet Sun Solar spectrum (Manson 1972)
unidentified line at 93.61 Å

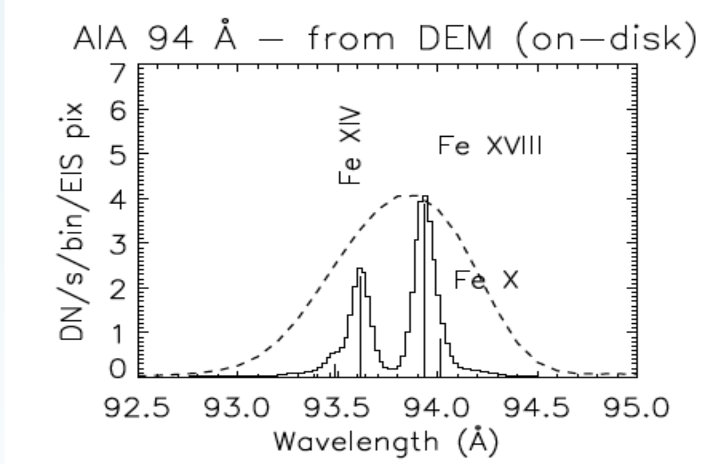

Fawcett Fe XIV: 91.27 Å

New identification of the 93.61 Å line with Fe XIV (Del Zanna 2012) confirmed by GRASP2K (Ekman+2017)

Soft X-rays → EUV,UV, infrared !

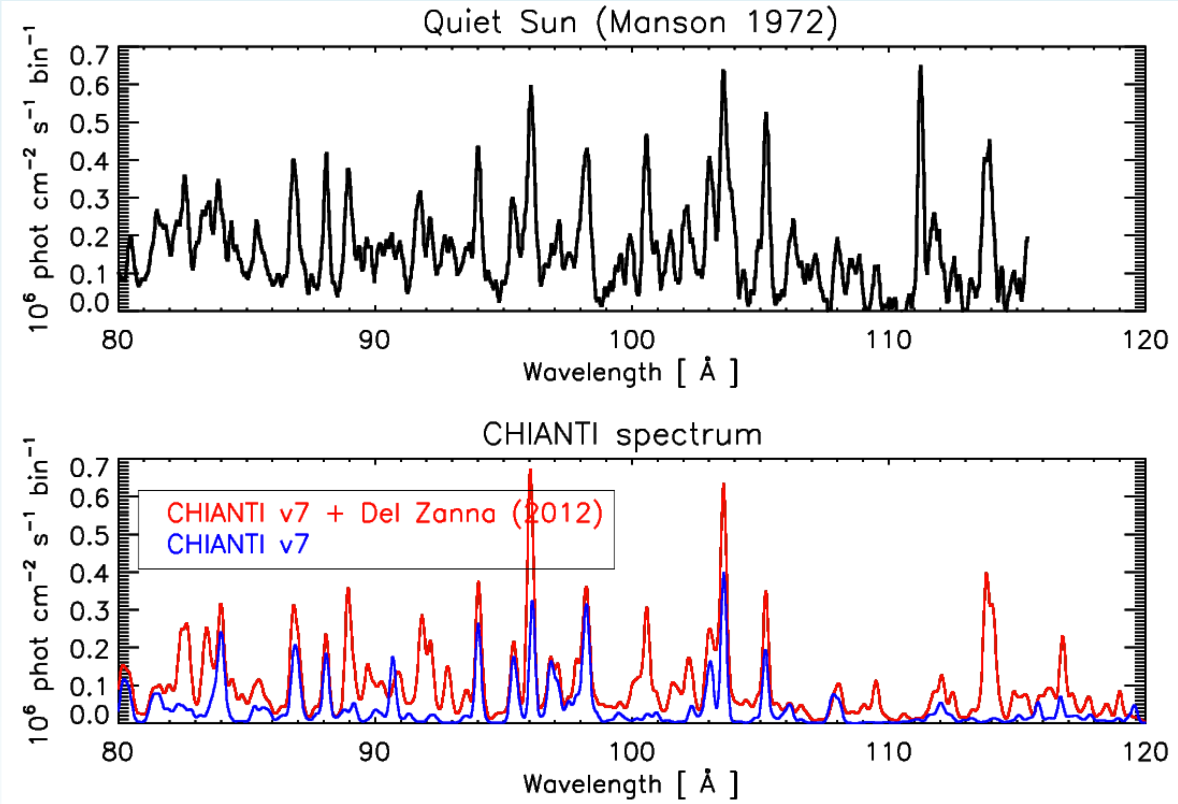

No scattering data was available for these transitions until a series of R-matrix calculations for Fe ions (Del Zanna+). Cascading from higher levels and increased cross-sections significantly increase the populations of the lower levels, affecting diagnostics in the EUV and intensities of the forbidden lines up to factors of 2, from the UV to the infrared

The soft X-rays and the forbidden lines

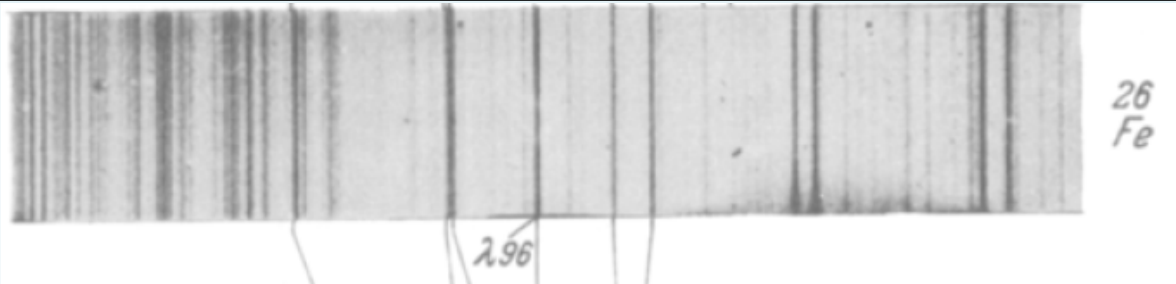

Edlen (1936)

Fe X identifications in the soft X-rays from Edlen in 1930's

New scattering calculations show stronger transitions, identified by Del Zanna (2012)

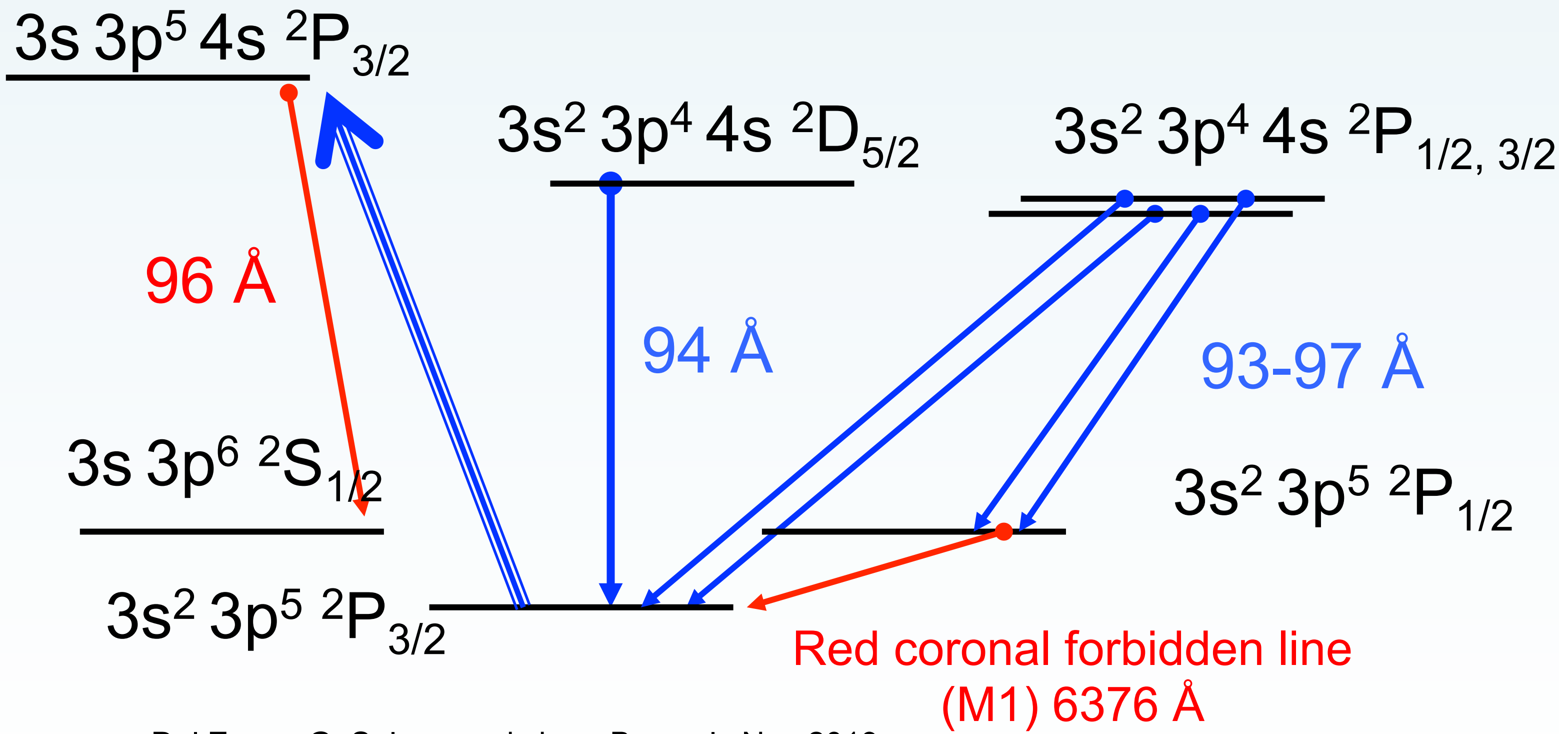

Fe XII

Del Zanna (2012): the population of the $3s^2\,3p^3\ ^2D_{5/2}$ is 50 % higher than previous models (Storey et al. 2005; Del Zanna & Mason 2005)

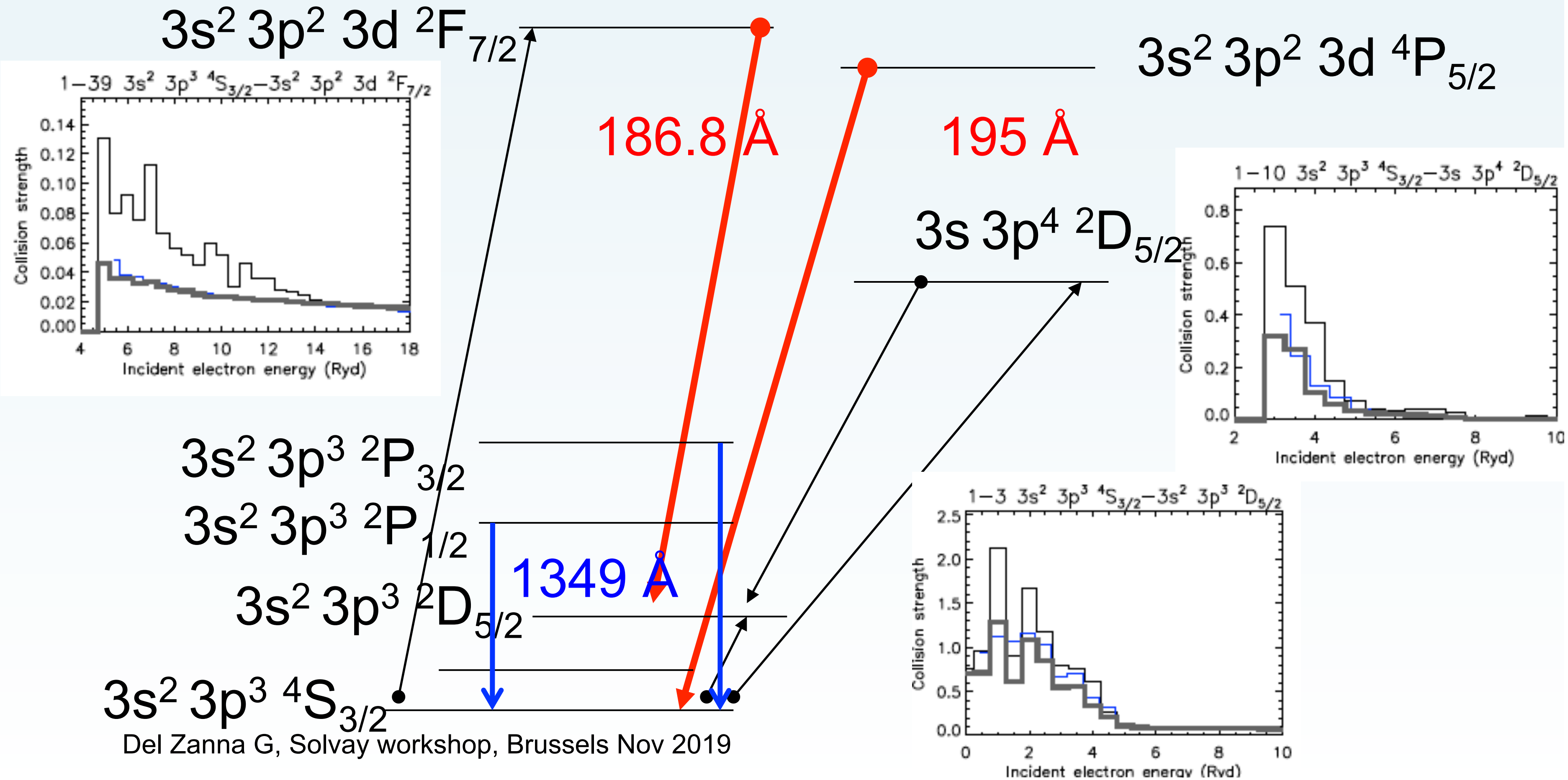

Fe XII

The new ion model reduces the densities from the EUV lines.

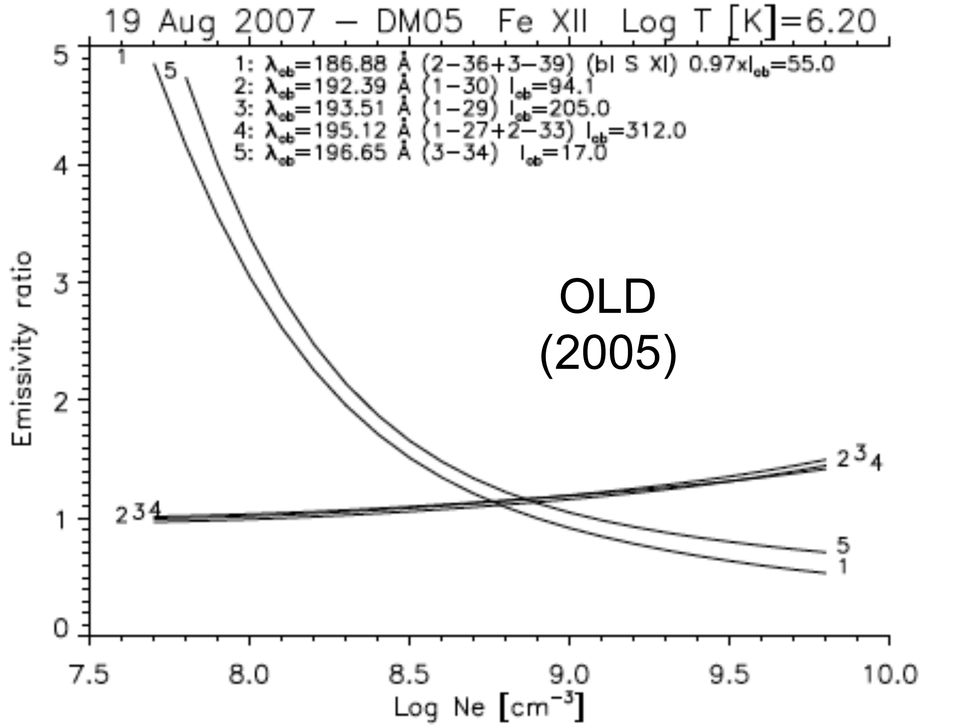

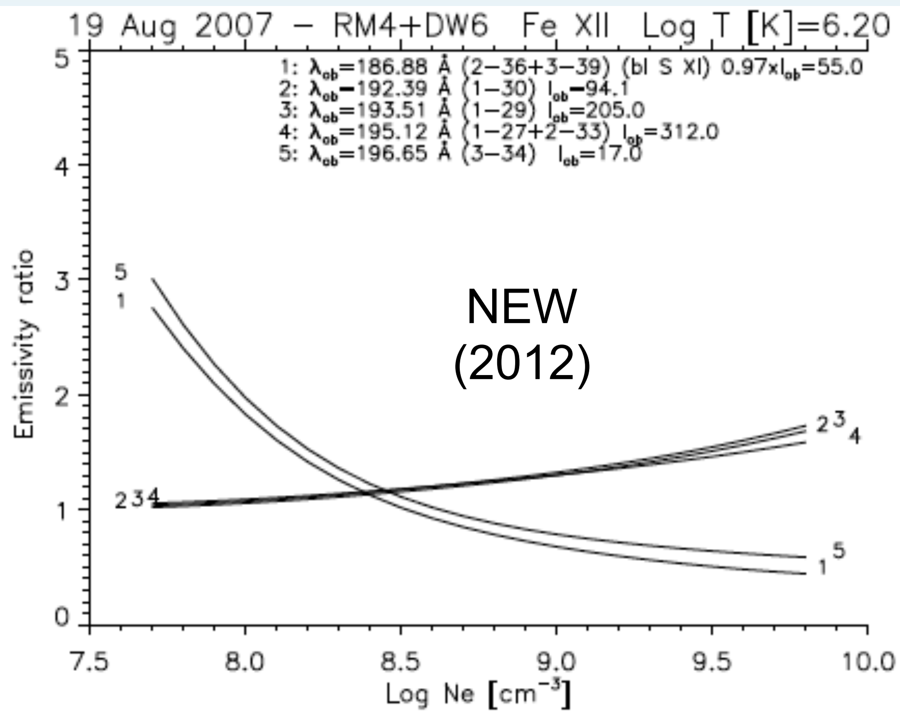

EUV High-resolution spectroscopy − Hinode EIS

1) 50% of the lines unidentified; factors of 2 problems in predicted intensities

Improvements in line ID using atomic rates and laboratory data:

Fawcett plates (EBIT Livermore useful) − **lack of availability of old lab data**

2) Calibration

3) Opacity effects

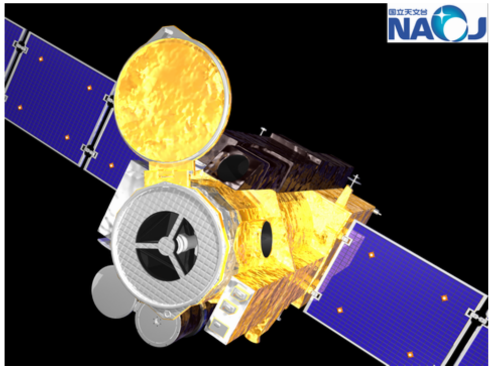

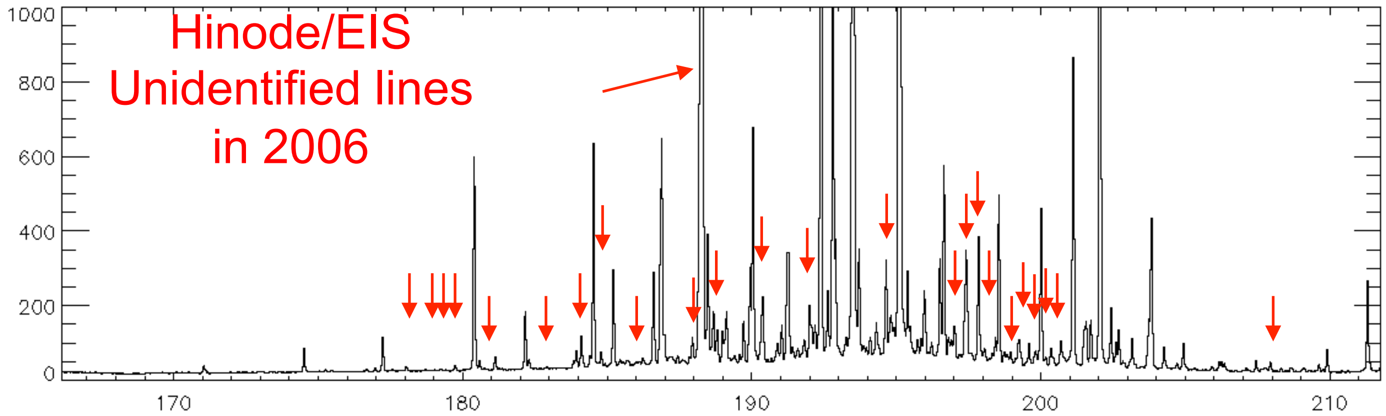

Mostly Fe VII-Fe XIV

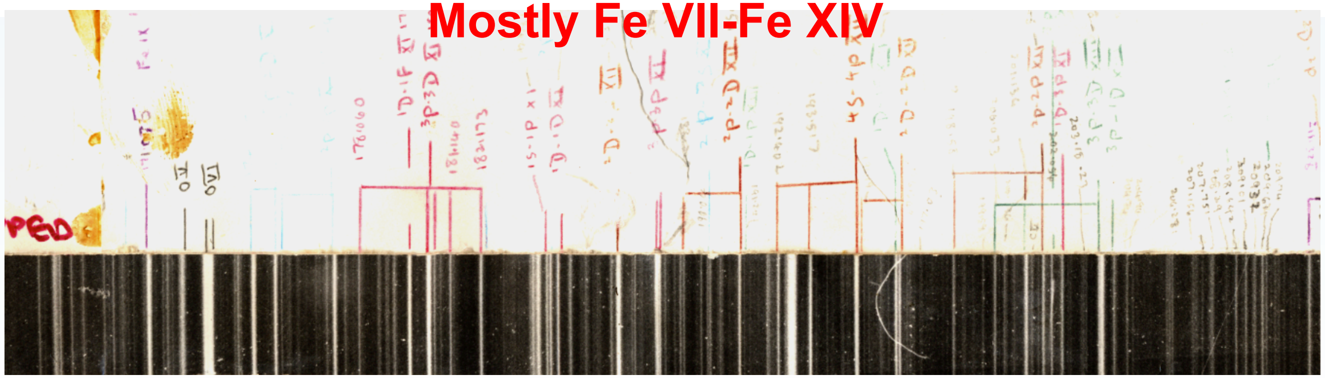

B.Fawcett 166 – 212 Angstroms

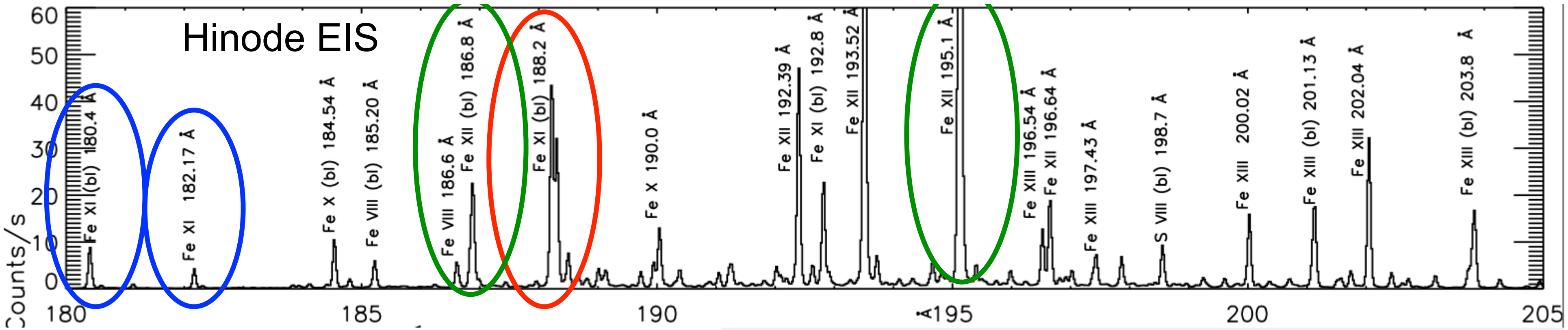

Gabriel et al.(1966)

i-*j*	λ_{exp} (Å)	λ_{obs} (Å)	ID	Diff. ID
6-103	168.929	? 168.929(10) Be76		
1-43	178.058	178.056(4) Be76	G66	
4-46	179.758	179.758(10) Be76	G66	
1-42	180.401	180.401(2) Be76 (bl)	G66	
2-44	180.594	180.595(4) Be76	F71	
3-44	181.130	181.131(10) Be76	G66	
2-43	182.167	182.167(2) Be76	G66	
4-45	184.793	184.793(10) Be76 (bl u)	FG66	
1-38	188.216	188.216(2) Be76	B77	F71 (188.299)
1-37	188.299	188.299(2) Be76	J93	B77(189.94)
2-41	189.123	189.123(4) Be76 (bl u)	B77	J93 (192.619)
3-41	189.711	189.723(5) N (bl)	B77	
1-36	190.382	190.382(5) N (bl u)	N	Be76 (S XI)
2-39	192.021	192.021(5) N (bl)	B77	
3-39	192.627	192.624(5) N (bl u)	B77	
2-38	192.813	192.811(5) N (bl O V, u)	F71	
3-37	193.512	- (bl Fe XII 193.509(2))		
4-41	198.538	198.555(10) Be76 (bl S VIII)	B77	Be76, J93
1-35	201.112	201.112(5) N (bl Fe XIII)	N	
4-39	201.734	201.734(10) Be76 (bl Fe XII)	B77	
1-34	202.424	202.424(10) Be76 (bl u)	N	B77 (201.575)
4-38	202.609	- (bl S VIII 202.608(10))		
4-37	202.705	202.710(10) Be76 (bl)		
1-30	206.169	206.169(10) Be76 (bl u)	N	
1-29	206.258	206.258(5) N	N	
2-34	207.751	207.749(5) N (bl u)	N	
2-33	209.771	209.771(5) N (bl u)		
1-20	234.730	234.73(2) D78	N	D78 (Fe XV)
1-18	236.494	236.494(10) Be76	N	
1-17	239.780	? 239.78(2) D78	N	
1-16	240.717	240.713(4) Be76 (bl Fe XIII)	N	
1-15	242.215	242.215(10) (bl) Be76	N	

Fe XI benchmark: Del Zanna (2010)
31 (out of 60) new line identifications,
later confirmed by GRASP2K
(Wang+2018)

Wang+ 2018

Key	Level	$E_{\rm MCDHF}$	$\Delta E_{\rm MBPT}$	$\Delta E_{\rm AS}$	$\Delta E_{\rm NIST}$	$\Delta E_{\rm D10}$
1	$3s^2\,3p^4(^3P)\ ^3P_2$	0	0	0	0	0
2	$3s^2\,3p^4(^3P)\ ^3P_1$	12663	-92	5	5	5
3	$3s^2\,3p^4(^3P)\ ^3P_0$	14365	-111	-59	-53	-59
4	$3s^2\,3p^4(^1D)\ ^1D_2$	37896	-331	-153	-152	-153
5	$3s^2\,3p^4(^1S)\ ^1S_0$	81125	51	-294	-310	-294
6	$3s\ 3p^5\ ^3P^o_2$	283710	-603	-159	-152	-159
7	$3s\ 3p^5\ ^3P^o_1$	293323	-793	-165	-165	-165
8	$3s\ 3p^5\ ^3P^o_0$	299356	-931	-193	-193	-193
9	$3s\ 3p^5\ ^1P^o_1$	362224	-1218	-378	-382	-378
10	$3s^2\,3p^3(^4S)\ ^4S\,3d\ ^5D^o_0$	387579	1488	-3357		-35
11	$3s^2\,3p^3(^4S)\ ^4S\,3d\ ^5D^o_1$	387749	1298	-3304		-23
12	$3s^2\,3p^3(^4S)\ ^4S\,3d\ ^5D^o_2$	387959	887	-3213		-19
13	$3s^2\,3p^3(^4S)\ ^4S\,3d\ ^5D^o_3$	388287	346	-3088		-19
14	$3s^2\,3p^3(^4S)\ ^4S\,3d\ ^5D^o_4$	389130	-16	97		97
15	$3s^2\,3p^3(^2D)\ ^2D\,3d\ ^3D^o_2$	413144	-301	-288		-288
16	$3s^2\,3p^3(^2D)\ ^2D\,3d\ ^3D^o_3$	415664	-524	-2371		-238
17	$3s^2\,3p^3(^2D)\ ^2D\,3d\ ^3D^o_1$	417325	577	-276		-276
18	$3s^2\,3p^3(^2D)\ ^2D\,3d\ ^3F^o_2$	423132	792	-288		-288
19	$3s^2\,3p^3(^2D)\ ^2D\,3d\ ^1S^o_0$	425681	-590	-2554		
20	$3s^2\,3p^3(^2D)\ ^2D\,3d\ ^3F^o_3$	426370	494	-348		-348
21	$3s^2\,3p^3(^2D)\ ^2D\,3d\ ^3F^o_4$	430719	104	-197		-197
22	$3s^2\,3p^3(^2D)\ ^2D\,3d\ ^3G^o_3$	449077	-44	-548		
23	$3s^2\,3p^3(^2D)\ ^2D\,3d\ ^3G^o_4$	450595	-179	-385		-384
24	$3s^2\,3p^3(^2D)\ ^2D\,3d\ ^3G^o_5$	452939	-447	-523		-523
25	$3s^2\,3p^3(^2D)\ ^2D\,3d\ ^1G^o_4$	459723	-356	-505		-505
26	$3s^2\,3p^3(^2P)\ ^2P\,3d\ ^1D^o_2$	466992	-234	-1518		
27	$3s^2\,3p^3(^2P)\ ^2P\,3d\ ^3D^o_1$	482156	-604	-1354		
28	$3s^2\,3p^3(^2P)\ ^2P\,3d\ ^3P^o_0$	482985	-225	-2286		
29	$3s^2\,3p^3(^2P)\ ^2P\,3d\ ^3P^o_1$	485354	-338	-2024		-524
30	$3s^2\,3p^3(^2P)\ ^2P\,3d\ ^3F^o_3$	485585	-102	-546		-546
31	$3s^2\,3p^3(^2P)\ ^2P\,3d\ ^3F^o_2$	486728	55	-1399		
32	$3s^2\,3p^3(^2P)\ ^2P\,3d\ ^3F^o_4$	486851	-340	-438		-438
33	$3s^2\,3p^3(^2P)\ ^2P\,3d\ ^3D^o_2$	489985	-156	-607		-607
34	$3s^2\,3p^3(^2P)\ ^2P\,3d\ ^3P^o_2$	494506	-325	-493	1584	-493
35	$3s^2\,3p^3(^2P)\ ^2P\,3d\ ^3D^o_3$	497953	-339	-718		-718
36	$3s^2\,3p^3(^2P)\ ^2P\,3d\ ^1F^o_3$	526154	-515	-894		-894
37	$3s^2\,3p^3(^2D)\ ^2D\,3d\ ^1P^o_1$	531598	-912	-528	-5118	-528

Solar coronal abundances?

Connection with heating processes (cf. Laming 2015, Living Review)
Useful for Solar Orbiter
Improved atomic data and models have changed completely the previously-accepted scenario (see Del Zanna & Mason Liv.Rev.).

SDO EVE: the solar quiet corona has photospheric abundances!

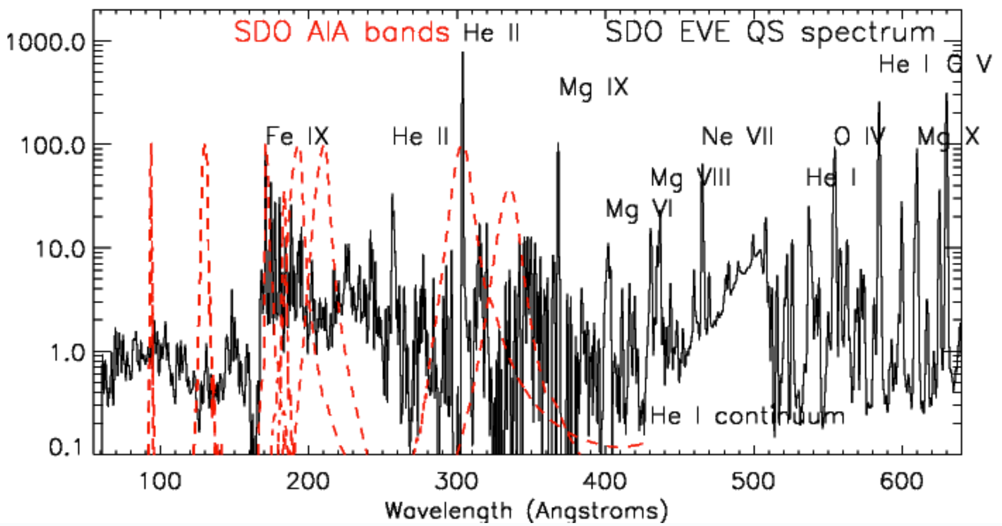

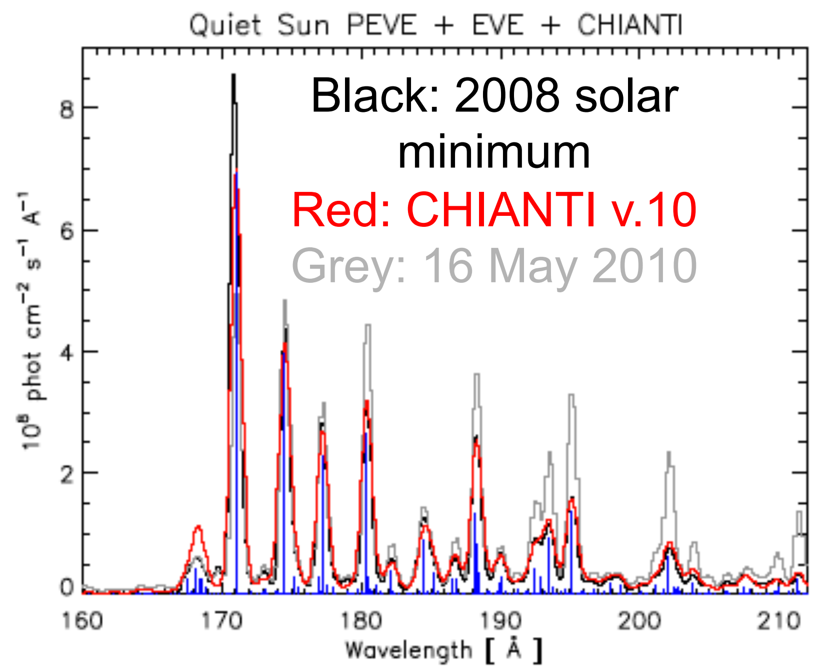

Del Zanna (2019, A&A)

Abundances in the TR: anomalous ions!

The strongest lines in the UV, from Li-like and Na-like ions are stronger (factors of 2-5) than predicted.

Si IV and C IV

Del Zanna+(2002): first to show that the problem is present also in stars (Hubble HST).

$$EMLoci = \frac{Iobs}{Ab(X)\ Gji(Te)}$$

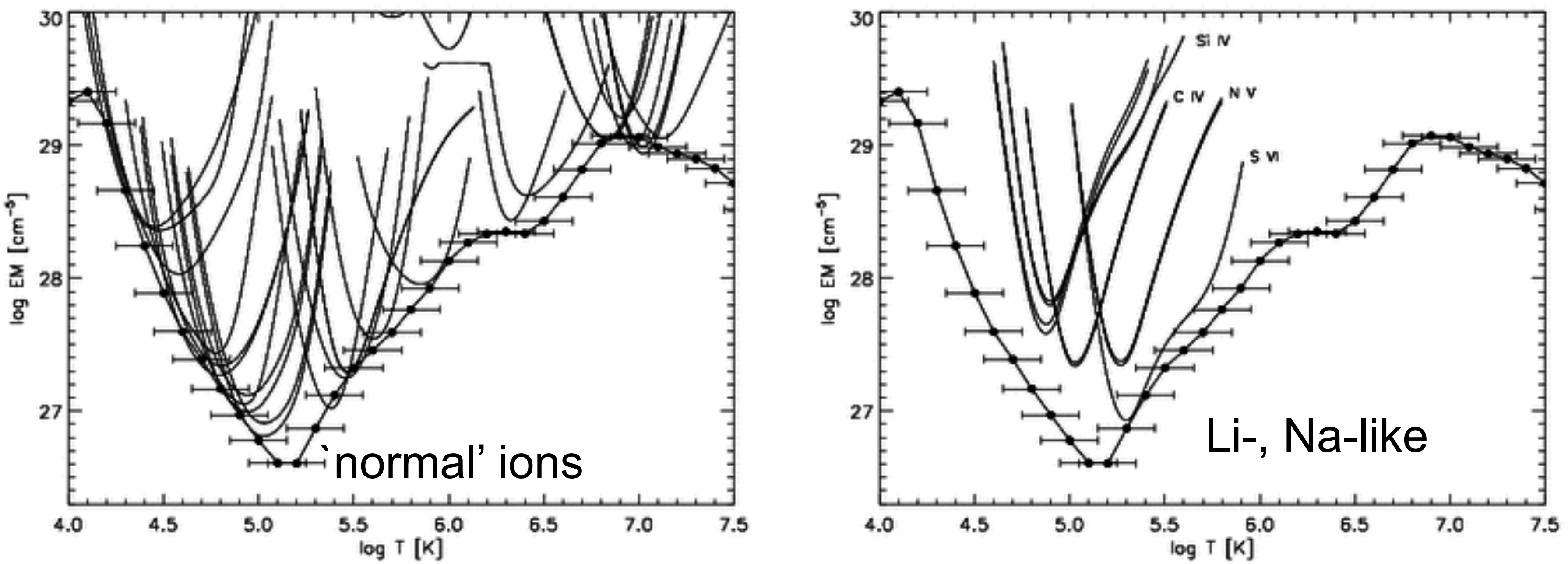

IRIS

NASA
SMEX

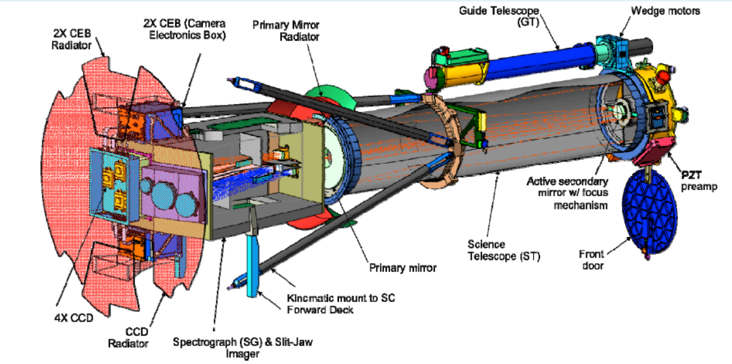

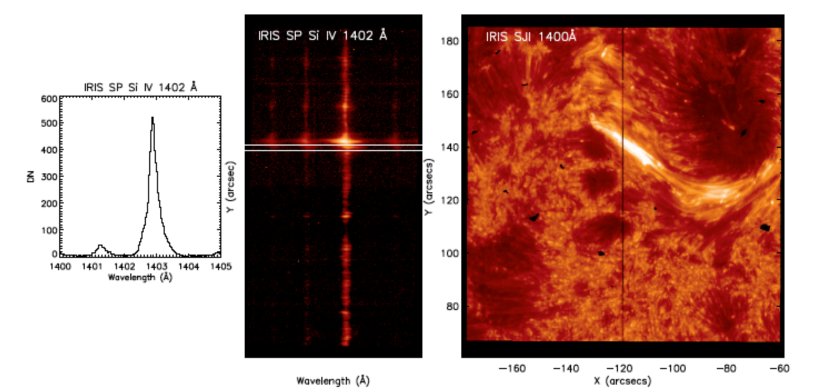

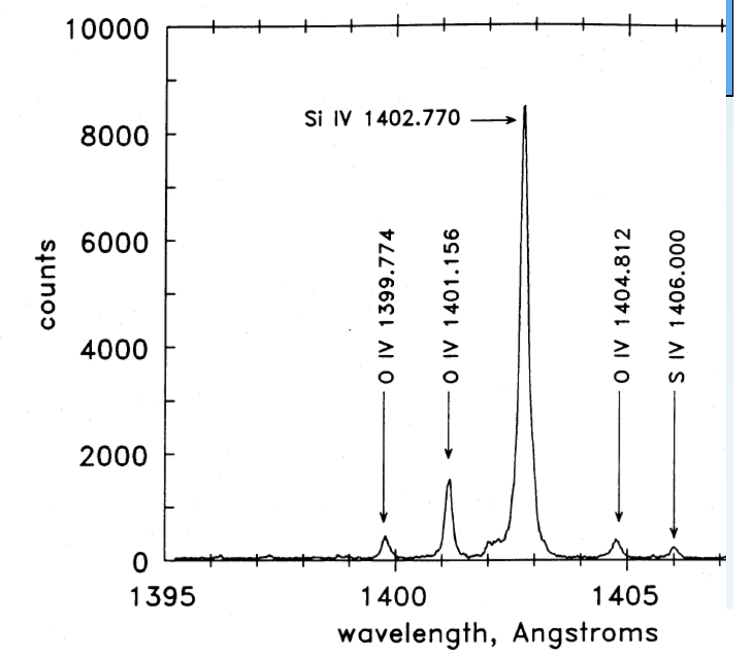

Maxwellian (black) and non-Maxwellian kappa distributions (colours)

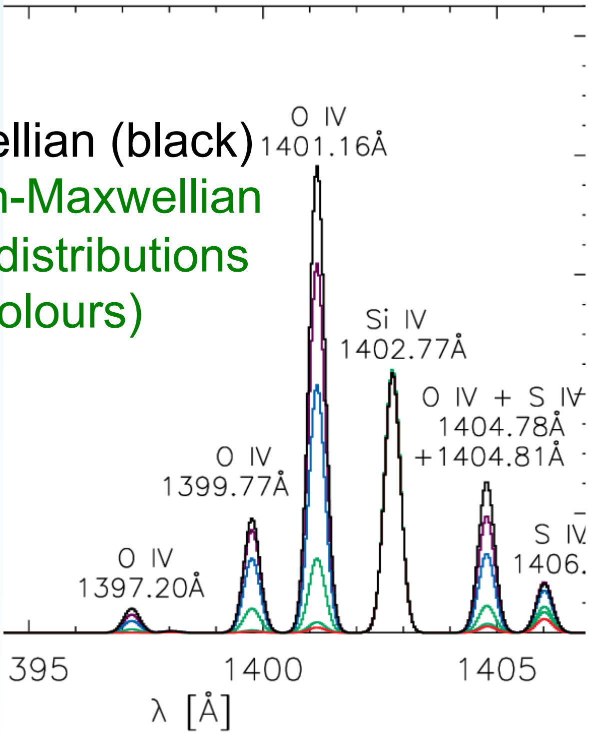

Anomalous Si IV intensity:

1) non-equilibrium ionisation (cf. Bradshaw, Del Zanna & Mason 2004)
2) Non-Maxwellian electrons (Dudik, Del Zanna et al. 2014)
3) But..

C-R Modelling: Level-Resolved

A new approach − a complete level-resolved collisional-radiative model

1) New: level-resolved CI from ground and metastable levels.
2) DR from ground and excited states from the DR-project (Badnell). Suppression at high Ne important (Burgess and Summers 1969)
4) (new) photo-ionisation from ground and excited levels
5) RR, Charge exchange, photo-excitation,etc.

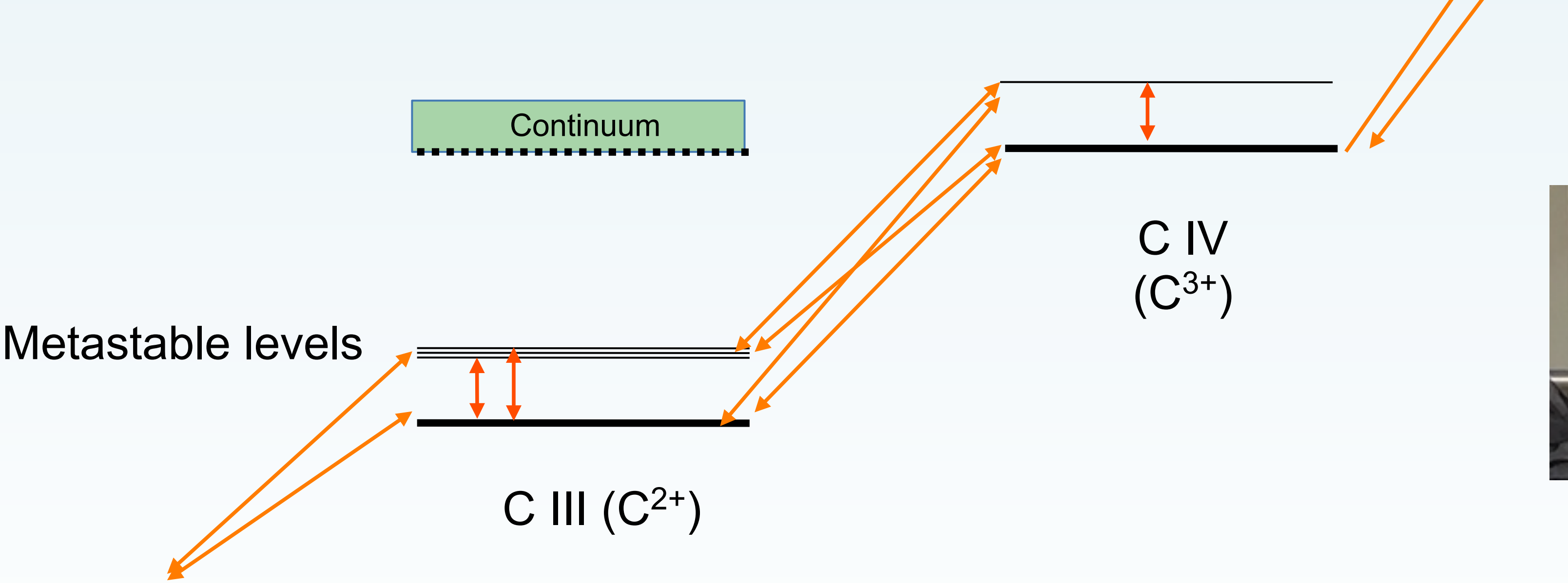

Del Zanna G, Solvay workshop, Brussels Nov 2019

Carbon

Dufresne & Del Zanna (2019, A&A): increase of C IV solar intensity by a factor of 2.5

Significant effects in high-density plasmas (e.g. AGN) and in Oxygen

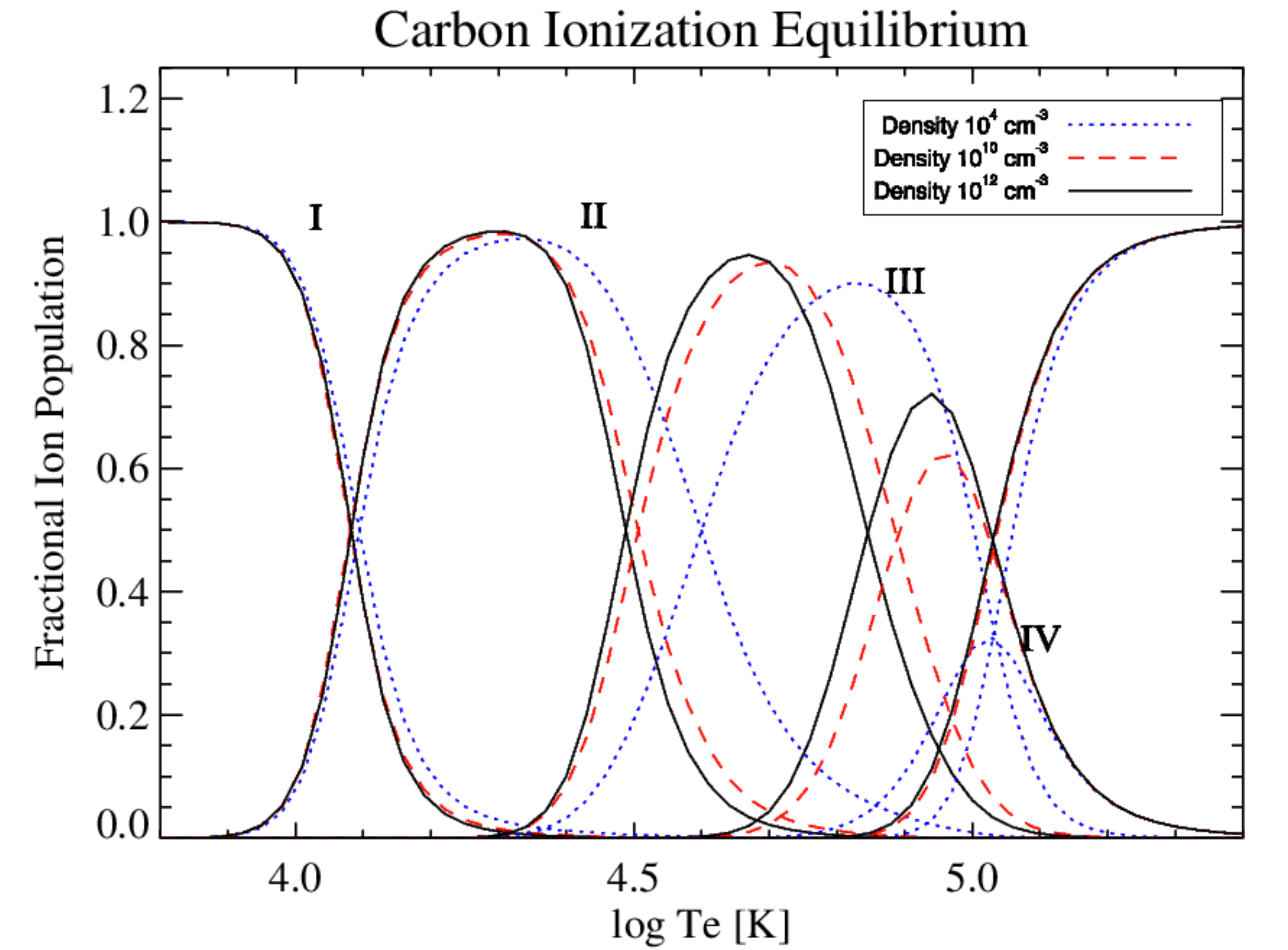

D

Relevant for Solar Orbiter

First ESA M-class, launch: Feb 2020. A suite of in-situ (as close as 0.3 AU) and remote-sensing instruments to study the solar wind.

Chemical abundances to trace the origin of the solar wind

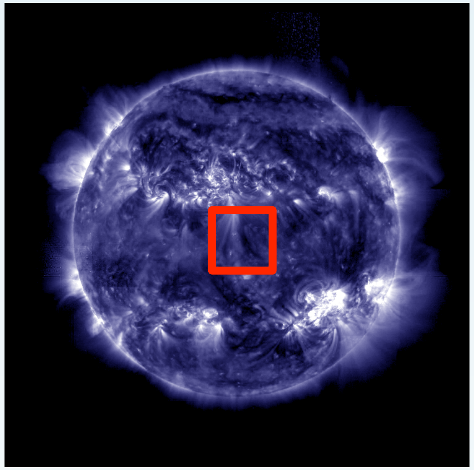

EUV images and magnetograms

SPICE spectrometer has two UV channels, mostly low-T lines affected by issues

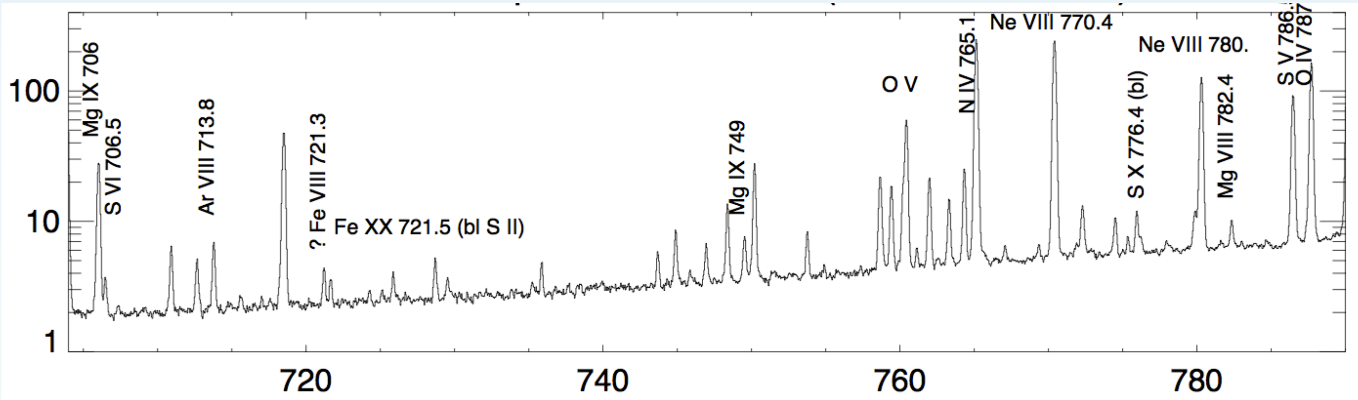

SUMER QS spectrum 972.5-1050 (Curdt et al 2001)

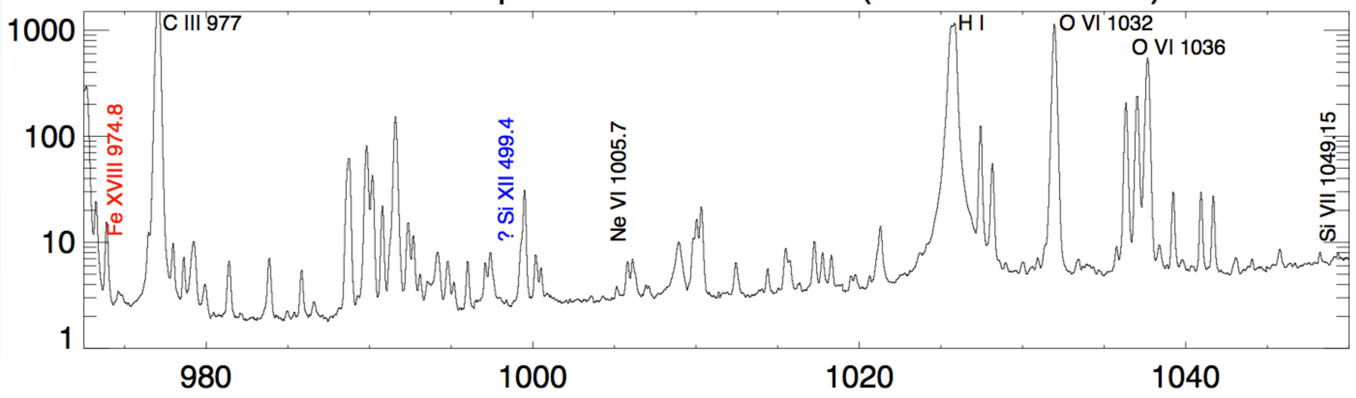

Del Zanna G, Solvay workshop, Brussels Nov 2019

DKIST: next-generation 4m solar telescope

First high-resolution spectroscopic observations (1-5 microns) to measure coronal magnetic field

First complete benchmark study (Del Zanna & DeLuca 2018)

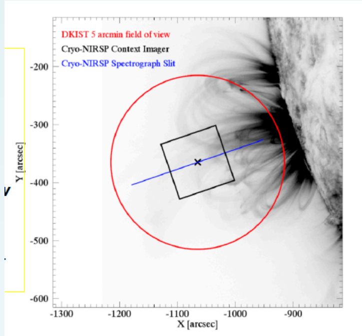

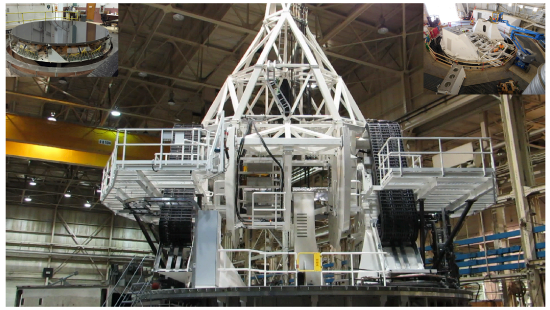

Only 300m+ USD

visible and NIR nearly unexplored !
Atomic rates for forbidden transitions need improvement

Mao+ poster

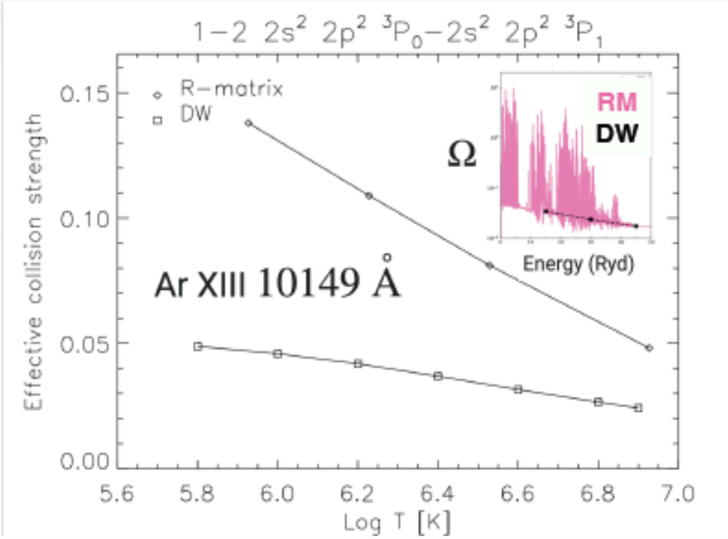

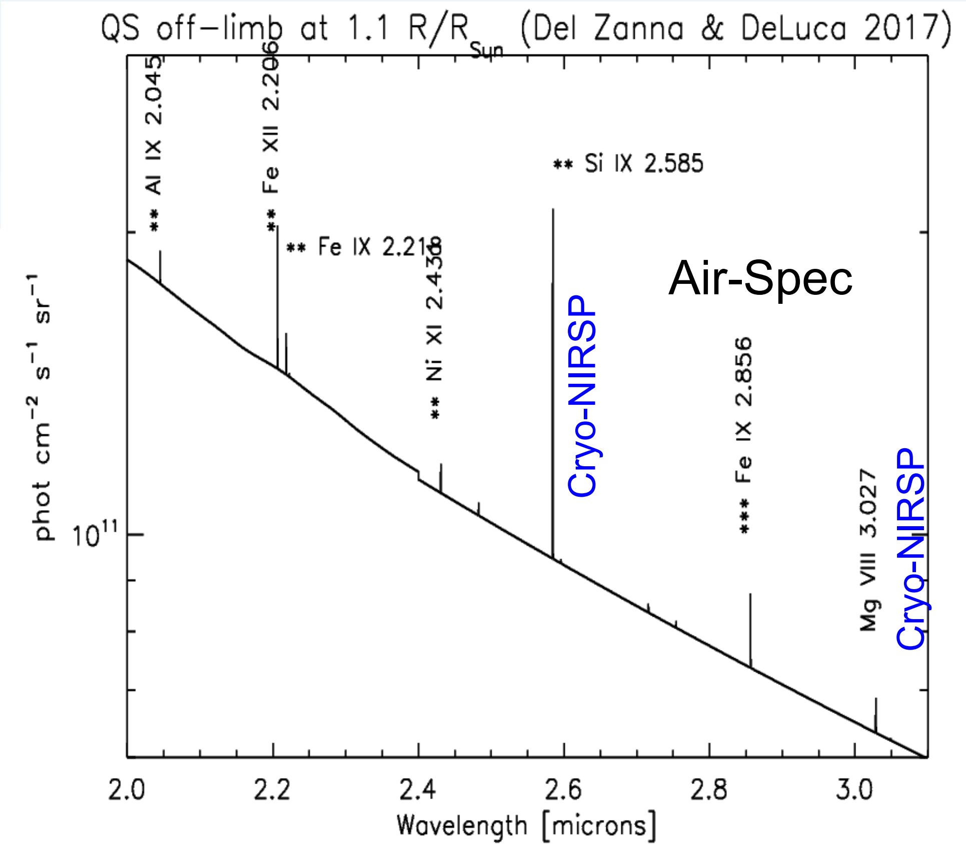

Del Zanna G, Solvay workshop, Brussels Nov 2019

Coronal forbidden lines - DKIST

Primary DKIST lines are Fe XIII and He I for density and B measurements. Issues:

1) New Fe XIII model (Del Zanna) requires a large number of levels
2) Modelling the photo-excitation is non-trivial
3) The He I collisional-radiative modelling is complex (work in progress)

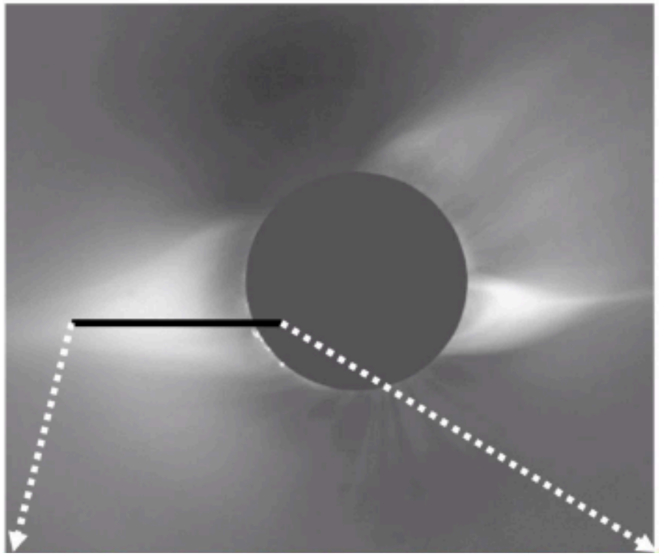

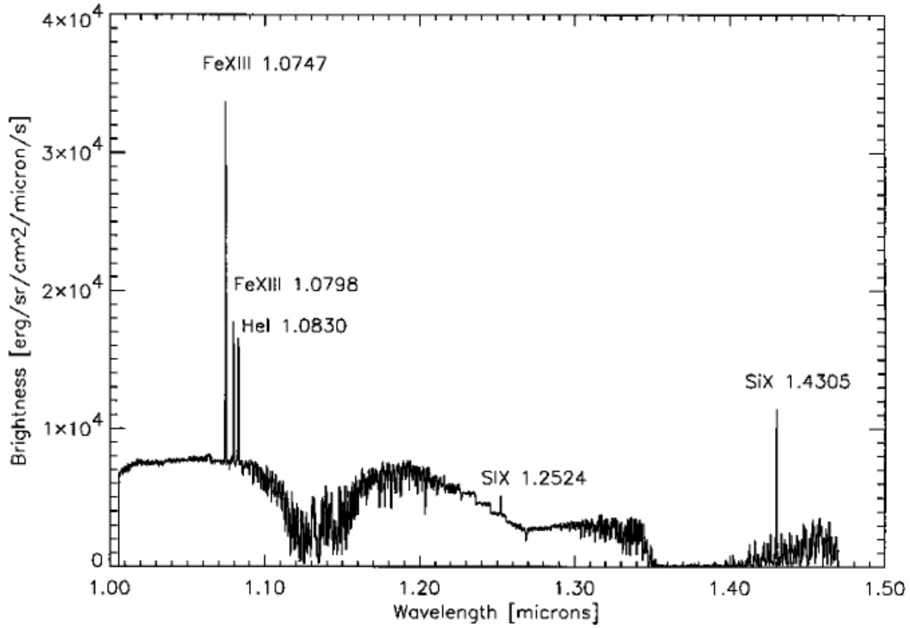

(Kuhn, Penn, and Mann 1996 – Putre Eclipse)

NIR coronal S abundance: photospheric!

Air-Spec: first near-infrared spectra (after Olsen+1971) 2017 eclipse from a high-altitude airplane

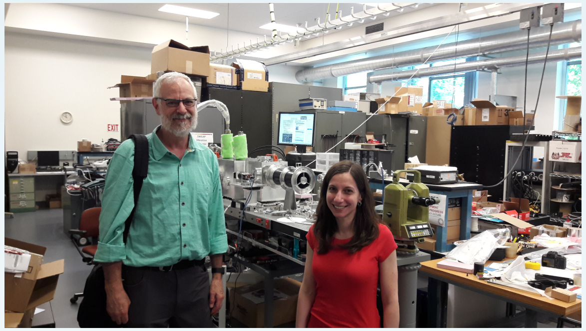

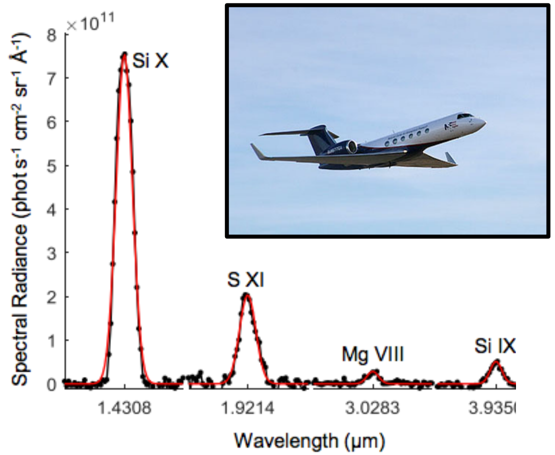

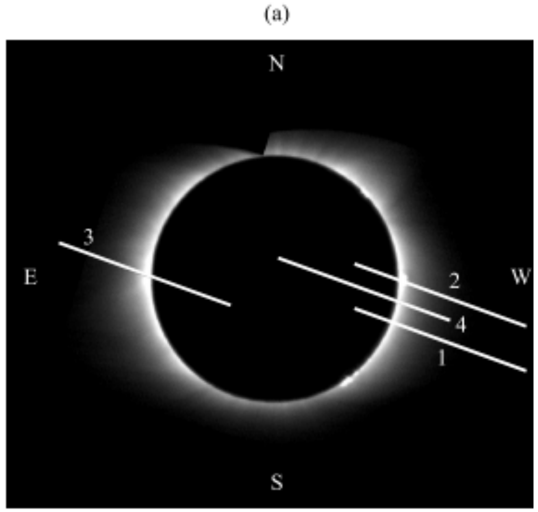

Incorrect Fe IX id (Samra,Judge+2018)

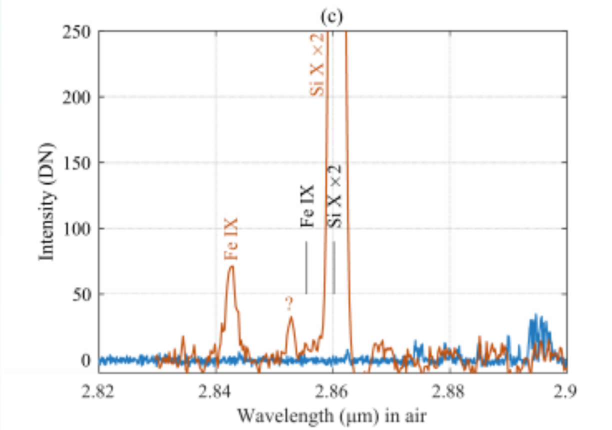

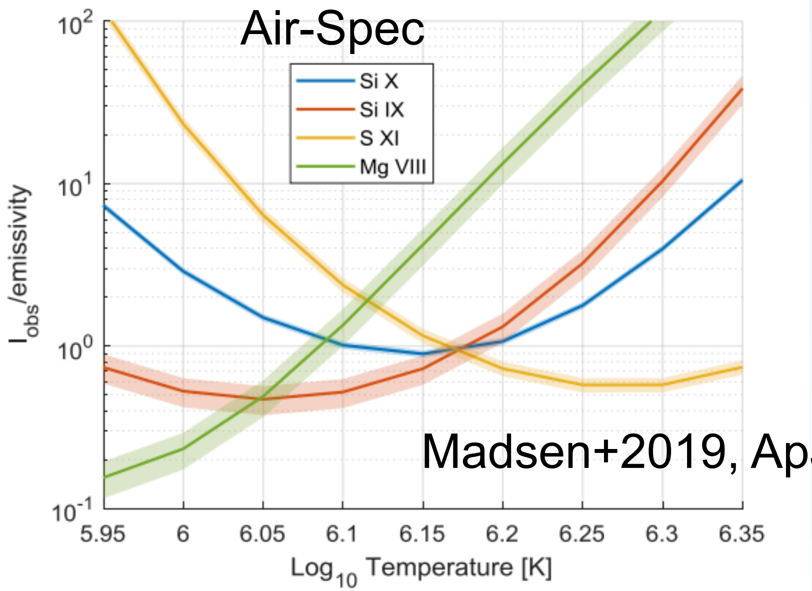

Madsen+2019, ApJ

nearly isothermal and photospheric abundances (Asplund+2009)

Conclusions

High-resolution spectral imaging is requiring improvements in atomic rates, line identifications, and proper modelling with more physical processes included.

Significant advances in atomic structure, more work on scattering and line ID needed.

The next challenge is to improve the modelling of the chromosphere-corona transition by including all processes (radiative transfer, time-dependent NLTE) for DKIST and Solar Orbiter